Volume 15 | Number 46 | 14 December 2019 | Pages 9379–9598

Soft Matter

rsc.li/soft-matter-journal

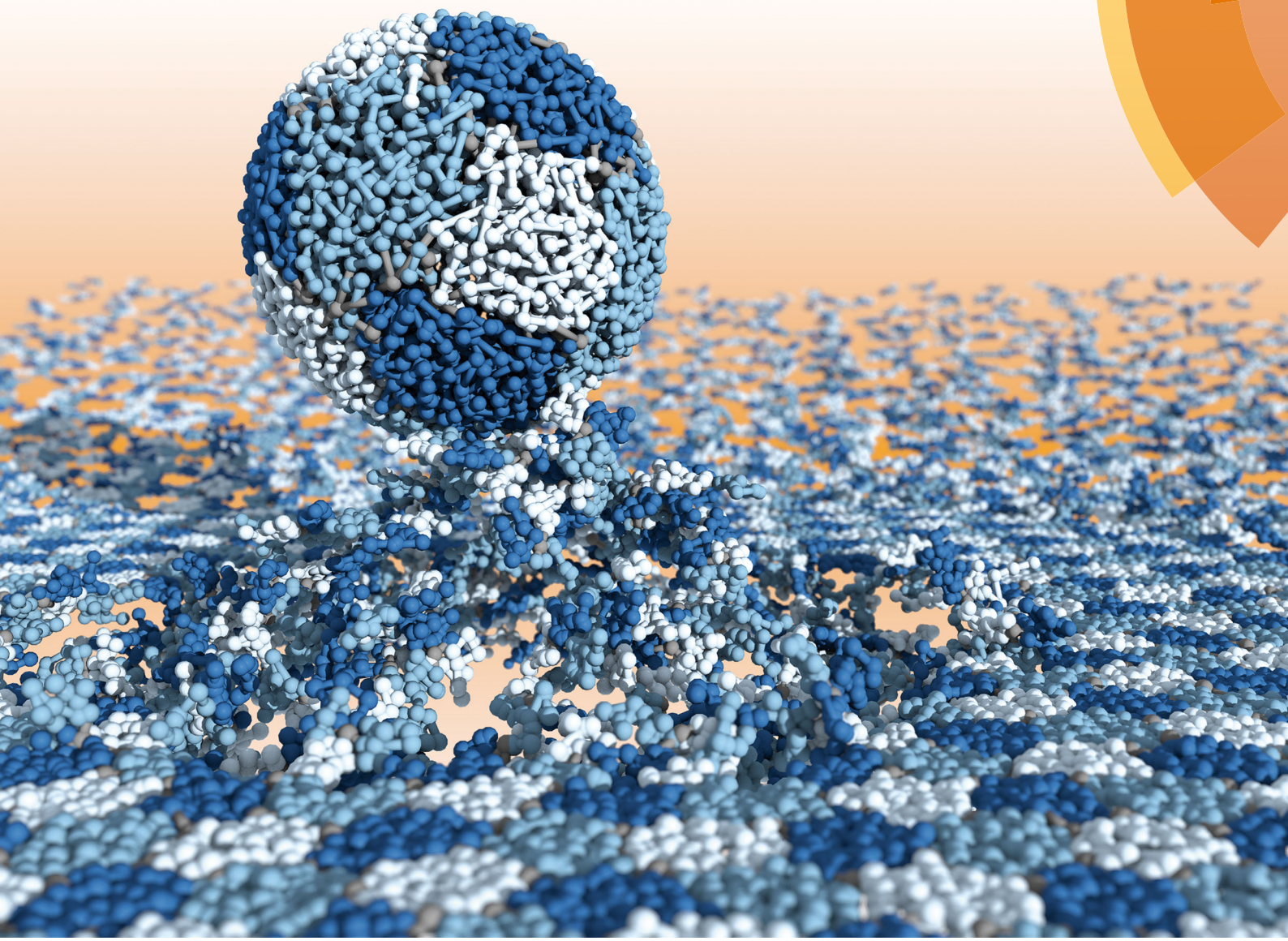

ISSN 1744-6848

ROYAL SOCIETY OF CHEMISTRY | Celebrating IYPT 2019

PAPER
Gerd E. Schröder-Turk, Jacob J. K. Kirkensgaard *et al.*
Patchy particles by self-assembly of star copolymers on a spherical substrate: Thomson solutions in a geometric problem with a color constraint

Soft Matter

PAPER

Check for updates

Cite this: *Soft Matter*, 2019, **15**, 9394

Patchy particles by self-assembly of star copolymers on a spherical substrate: Thomson solutions in a geometric problem with a color constraint†

Tobias M. Hain, [ab] Gerd E. Schröder-Turk *[abc] and Jacob J. K. Kirkensgaard *[c]

Received 18th July 2019,
Accepted 29th September 2019

DOI: 10.1039/c9sm01460h

rsc.li/soft-matter-journal

Confinement or geometric frustration is known to alter the structure of soft matter, including copolymeric melts, and can consequently be used to tune structure and properties. Here we investigate the self-assembly of ABC and ABB 3-miktoarm star copolymers confined to a spherical shell using coarse-grained dissipative particle dynamics simulations. In bulk and flat geometries the ABC stars form hexagonal tilings, but this is topologically prohibited in a spherical geometry which normally is alleviated by forming pentagonal tiles. However, the molecular architecture of the ABC stars implies an additional 'color constraint' which only allows even tilings (where all polygons have an even number of edges) and we study the effect of these simultaneous constraints. We find that both ABC and ABB systems form spherical tiling patterns, the type of which depends on the radius of the spherical substrate. For small spherical substrates, all solutions correspond to patterns solving the Thomson problem of placing mobile repulsive electric charges on a sphere. In ABC systems we find three coexisting, possibly different tilings, one in each color, each of them solving the Thomson problem simultaneously. For all except the smallest substrates, we find competing solutions with seemingly degenerate free energies that occur with different probabilities. Statistically, an observer who is blind to the differences between B and C can tell from the structure of the A domains if the system is an ABC or an ABB star copolymer system.

1 Introduction

The self-assembly of linear diblock copolymers and their phase diagram is nowadays well understood.[1–3] By contrast, the study of the phase behaviour of more complex copolymer architectures, like grafts or stars,[4] remain incomplete, due to the larger parameter space and, hence, a larger variety of possible structures.[2,3,5–7] Here we consider ABC 3-miktoarm star terpolymers, henceforth called ABC star copolymers. These are copolymers which consist of three linear chains connected at a central grafting point,[3,4,8,9] as shown in Fig. 1 or Fig. 2. These star copolymers can be synthesized so that the three arms are immiscible; herein we refer to the three polymeric species as colors: blue, yellow and red. When this immiscibility drives the

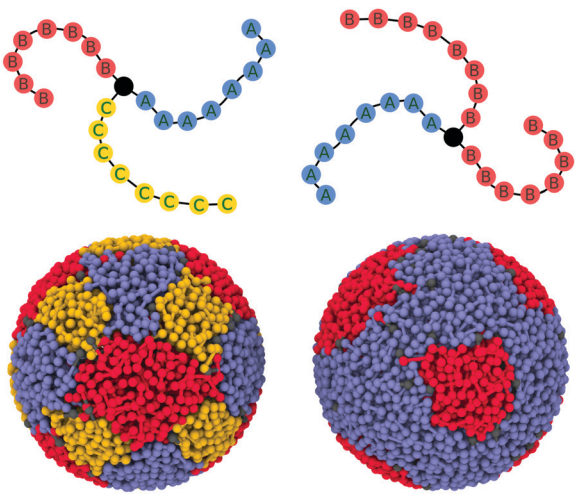

Fig. 1 Polymeric self-assembly of ABC and ABB star copolymers on a spherical substrate. Top panel: Schematic visualization of coarse grained models of ABC and ABB star copolymers used for the DPD simulations. Bottom panel: Snapshots of simulations comprising ABC and ABB star copolymers. Polymer arms of identical color agglomerate into patches. The ABC system creates a three colored tiling of the sphere, whereas the ABB system builds a single tiling made up of only A-type patches in a B-type matrix.

[a] *College of Science, Health, Engineering and Education, Mathematics and Statistics, Murdoch University, 90 South Street, 6150 Murdoch, Western Australia, Australia. E-mail: G.Schroeder-Turk@murdoch.edu.au*

[b] *Physical Chemistry, Department of Chemistry, Lund University, P.O. Box 124, 221 00 Lund, Sweden*

[c] *Department of Food Science, University of Copenhagen, Rolighedsvej 26, 1958 Frederiksberg, Copenhagen, Denmark. E-mail: jjkk@food.ku.dk*

† Electronic supplementary information (ESI) available. See DOI: 10.1039/c9sm01460h

This journal is © The Royal Society of Chemistry 2019

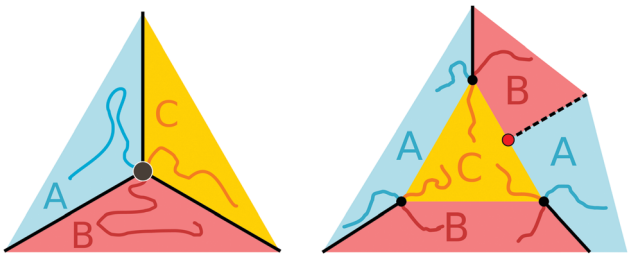

Fig. 2 Structural constraints imposed by polymer architecture: the color constraint. Left panel: Since the three different polymer arms making up domains are bonded at a central junction bead (grafting point), the latter must sit on points or lines where three different domains meet so that each arm may extend in a domain of its species. Right panel: For tiling patterns, this results in the so-called color constraint: only polygons with an even number of edges are allowed, where the types of all adjacent polygons alternate. The figure illustrates this: if a polygon with an uneven number of edges is attempted to be formed, a new interface (dashed line) and grafting point (red point) is introduced by the architecture of the stars, resulting in an even polygon.

moieties to micro-phase separation, the arms of equal species will agglomerate into domains, which will self-assemble into complex structures. Considerable amount of work has been put towards the investigation of one type of these structures: columnar phases whose cross-sections are planar tiling patterns.[10–20]

A distinguished and important feature of ABC star copolymers is that all structures arising from these molecules must be compatible with the special architecture of the latter:

1. The grafting points form triple lines[13] where three different domains meet, which, in cross-section, corresponds to vertices of the tiling pattern.

2. Any given patch of a given color (*e.g.* yellow), must be surrounded by an alternating sequence of patches of the other colors (*e.g.* blue and red). The number of these surrounding patches must then be even.[12]

For more details see Fig. 2. In this article we will refer to constraint 2 as the color constraint.

If the star copolymers are chosen symmetrically, *i.e.* all arms have equal length, and with equal interaction strength between the arms, a hexagonal columnar phase is formed where a cross section perpendicular to the columns yields a planar 3-colored honeycomb pattern which we here consider as the 'ground state' of the system.[10–13,16,19,21] The hexagonal tiling can be tuned into a large variety of tilings by varying the length of one of the three arms.[10,12,19] However, all these tilings consist of vertices of order three only, which is enforced by the molecular architecture of the star copolymers.

Apart from changing the chemical composition or interactions of the polymers, another way to tune structures is by geometric confinement. A simple analogy illustrates this fundamental geometric concept: the peel of an orange for example cannot be confined to a flat plane, without tearing or deforming it. This also applies for the star polymers: the optimal free energy configuration they form in the plane, the regular honeycomb, cannot be fitted on a spherical substrate without distorting the planar pattern.

Unlike the restriction of polymers to a thin film, the confinement to curved geometries, like spheres, does not only impose the constraint of physical confinement onto the polymers, but also introduces curvature to the system. This alters the shape and structure of the space available to the polymer melt which can enforce or prohibit some structures to form. Such curvature-related effects have been described for multiple self-assembly systems.

Several articles report on the influence of curvature on hexagonal particle orders on surfaces with positive and negative curvature, both using experiments[22–27] and simulations.[24,28,29] Two dimensional tilings can be created from these particle assemblies by assigning each particle a polygon where the number of edges coincides with its coordination number, which is the number of neighbouring particles. This process is equivalent to computing a Voronoi diagram of the particles. While these particles would arrange in a hexagonal order in a plane, and therefore, form a perfect hexagonal tiling, defects in this patterns were found after the particles self-assembled on curved surfaces.

Zhang *et al.*[30] found similar defects in the self-assembly of AB diblock copolymers confined to a spherical substrate using numerical methods to solve the Landau–Brazovskii theory. For cylinder forming diblocks, the cylinders distributed over the surface of the sphere in a generally hexagonal order, however, 5-fold defects were found. For larger systems, scars of connected 5- and 7-fold defects occur. These scars were previously found by Chantawansri *et al.*[31] in their studies about AB diblock copolymers on spherical substrates using SCFT. They furthermore found that the number of cylinders depends on the radius of the spherical substrate.

These defects have a fundamental mathematical origin: the different topologies of the confining surface. Each tiling and polyhedra (and topological equivalents) have an intrinsic property, the Euler characteristic χ, describing its topological type.[32–34] An Euler characteristic of $\chi = 2$ corresponds to an object that is a single component without any handles or cavities, such as the sphere. A given tiling can only tessellate a surface of the same topological space, therefore surfaces having the same Euler characteristic as the tiling.[33] A planar, periodical hexagonal tiling has $\chi = 0$, as does a torus. Therefore the hexagonal tiling can be mapped onto the latter. When a hexagonal lattice is forced onto an incompatible curved surface, as for example a sphere with $\chi = 2$, the mismatch leads to 'geometric frustration': the hexagonal lattice is incompatible with the topology of the substrate. To cope with this incompatibility defects occur in the hexagonal order.

To check if a tiling is compatible with a sphere, Euler's formula can be used, which reads in case of a sphere:[32,34]

$$\chi = V - E + F = 2 \tag{1}$$

where V, E, F is the number of vertices, edges and facets in the tiling. If a tiling fulfills this condition, it can be mapped onto a sphere without defects. In our case, where tilings are generated by ABC star copolymers, the color constraint can be incorporated into eqn (1). Since only vertices where three edges meet are allowed, each edge is shared by two and each vertex by three facets (see also Fig. 2). In this case, eqn (1) can then be expressed in terms of the number of polygons in the tiling:

$$\chi = \sum_i \left(\frac{i \cdot n_i}{3} - \frac{i \cdot n_i}{2} + n_i \right) = \sum_i \left(1 - \frac{i}{6} \right) n_i = 2 \tag{2}$$

where n_i is the number of polygons with i edges in the tiling. This equation easily shows that a hexagonal tiling is incompatible, since the term in the brackets equals zero for $i = 6$. Therefore polygons with a different number of edges need to be introduced to fulfil the equation. One solution to eqn (1) for the sphere is the arrangement of 12 pentagons to an icosahedron. Since the left side of eqn (1) vanishes for hexagons, an arbitrary number of the latter can be added to the 12 pentagons and the topology will not change. A well-known configuration is the soccer ball, consisting of 12 pentagons and 20 hexagons. Apart from investigations of particles from polymer systems, abstract systems with topological defects were investigated analytically.[33,35–37] Here the behavior of abstract disclinations from the crystalline state, for example particles with 5 neighbours in an otherwise hexagonal lattice, was investigated using free energy calculations. The results agree with the results found in the physical particle and polymer systems: the favoured state are 12 5-fold disclinations, also the above mentioned scars (connected disclinations) are found.

A very prominent problem of ordering on a sphere is the so-called Thomson problem. It was formulated by J. J. Thomson in 1904 in the context of his atomic model. The Thomson problem is the search for the minimal energy configuration of n repelling electrons, all of the same negative charge $-e$, on a spherical surface.[38] The resulting arrangement of electrons and their symmetries[39–43] has been found in many seemingly unconnected problems, as for example in the design of protein virus capsides,[44–46] the construction of fullerens and nanotubes,[47] in more generalized Thomson problem versions,[48] but also in connection with polymeric self-assembly where it was stated that the cylinders in the cylindrical phase of AB diblock copolymers on a spherical substrate arrange on the sphere as particles in the Thomson problem would.[31] To reach the minimal energy solution, the optimal coordination number of a single electron is six, however, due to the geometric frustration defects in the hexagonal order must occur, as explained above.[49] For our system, it is useful to interpret the electron positions of the Thomson problem solutions as vertices of a polyhedra. The graph of its dual polyhedron is a tiling of the sphere, where each electron is assigned a tile whose number of edges is equivalent to the coordination number of the corresponding electron. A solution of the Thomson problem, henceforth called a Thomson solution, can therefore be described and labeled by its dual lattice, see Table 1.

In conclusion, using ABC star copolymers confined to a spherical shell as a model system enables the simultaneous study of two different constraints: geometric frustration and the influence of the color constraint. To investigate the effects of each on their own, a strategy is needed to switch one of them on and off. This is accomplished by using two different kind of star molecules, the aforementioned ABC stars and ABB star molecules, see right panel in Fig. 1. These only differ to the ABC stars in that two arms are of the same species. Thus the color constraint can be eliminated, since the grafting points of the ABB stars can move freely across the interface between A and B type domains. The A type domains, which are the tiles in the resulting tiling, can then freely move around in a B type matrix.

Table 1 Solutions of the Thomson problem for systems with up to 12 electrons described as spherical tilings. The table shows the number of n-gons and the Schläfli symbol for the dual lattice of a solution of a N-electron Thomson problem. A Schläfli symbol[12,69,70] is a set of l numbers $[k_1,k_2,\ldots k_l]$ denoting that a vertex is adjacent to l tiles with k_l edges respectively (see also right pane in Fig. 5). The Schläfli symbol for an entire tiling just lists all different types of occurring vertices, see Fig. 5. The symbols to the left relates to the textures in Fig. 6

			Number of tiles with					
	N	Schläfli symbol	1 Edges	2	3	4	5	6
	2	[1.1]	2					
	3	[2.2.2]		3				
	4	[3.3.3]			4			
	5	[3.4.4]			2	3		
	6	[4.4.4]				6		
	7	[4.4.5]				5	2	
	8	[[4.4.5], [4.5.5]]				4	4	
	9	[[4.5.5], [5.5.5]]				3	6	
	10	[[4.5.5], [5.5.5]]				2	8	
	11	[[4.5.5], [4.5.6], [5.5.5], [5.5.6]]				2	8	1
	12	[5.5.5]					12	
		Non-Thomson						
		Invalid						

2 Methods

2.1 Dissipative particle dynamics of star copolymers

Dissipative Particle Dynamic (DPD) simulations are used to find equilibrium configurations of the polymer systems. DPD simulations[50,51] are a type of molecular dynamic simulations designed for coarse grained models of molecules, which makes it a natural fit for polymer melts.[11,21,52,53] As all molecular dynamics simulations, the DPD method is based on the forward integration of Newton's equation of motion in time for each particle i:

$$\frac{\mathrm{d}^2\mathbf{x}_i}{\mathrm{d}t^2} = \frac{1}{m}\cdot\mathbf{F}_i$$

In our case, a particle is a single bead in the polymer arms (see Fig. 1), where each bead may represent many atoms. A symmetric star copolymer then consists of a center particle with three connected arms, each consisting of a chain of bonded particles. A schematic representation of such a coarse grained polymer is shown in Fig. 1.

We use the simulation package HOOMD-BLUE[54–56] to perform our simulations. We will only briefly discuss the parameters used at this point, for details on the implementation we refer to ref. 57 and the documentation of the HOOMD-BLUE package.[58] In this simulation package all units are given based on three reference units (distance $\mathscr{D}$, energy $\mathscr{E}$ and mass $\mathscr{M}$) which can be chosen arbitrarily. All other units, for example a force, can be derived from these units, for more details we refer to the HOOMD-BLUE manual.[58] In the course of this article, all given values are given in

This journal is © The Royal Society of Chemistry 2019

terms of these reference units unless stated otherwise. The package implements the DPD method following the formulation of ref. 51 and 57. Here the force on particle i is given as

$$\mathbf{F}_i = \sum_{i \neq j} \left(\mathbf{F}_{ij}^{\mathrm{C}} + \mathbf{F}_{ij}^{\mathrm{D}} + \mathbf{F}_{ij}^{\mathrm{R}} \right)$$

where the sum is over all particle pairs within a cutoff radius $r_c = 1$ around the i-th particle. The force consists of three contributions: a conservative force $\mathbf{F}_{ij}^{\mathrm{C}}$ representing the repulsive interactions between the particles, a dissipative force $\mathbf{F}_{ij}^{\mathrm{D}}$ and a random force $\mathbf{F}_{ij}^{\mathrm{R}}$. The latter two act as a thermostat to keep the temperature of the system constant. Since a thermostat is a built-in feature of the DPD interactions, the system is technically advanced as a *NVE* ensemble using a standard velocity-Verlet step algorithm, although it is effectively a *NVT* ensemble. The conservative force is 0 only for $r_{ij} \geq r_c$ and is otherwise given by

$$\mathbf{F}_{ij}^{\mathrm{C}} = a_{ij} \left(1 - \frac{r_{ij}}{r_c} \right) \hat{\mathbf{r}}_{ij} \tag{3}$$

where a_{ij} is the maximum repulsion between two particles and therefore a measure of the interactions strength, $\mathbf{r}_{ij} = \mathbf{r}_i - \mathbf{r}_j$ and $\hat{\mathbf{r}}_{ij} = \mathbf{r}_{ij}/|\mathbf{r}_{ij}|$. The interactions between two particles of the same species is given as $a_{ii} = 75\frac{k_{\mathrm{B}}T}{\rho}$, where ρ is the number density and $k_{\mathrm{B}}T$ the temperature in the polymer melt. The interaction parameters can be mapped onto the well established Flory–Huggins interaction parameter χ_{ij}[59,60] used in polymer science using $a_{ij} = a_{ii} + 3.268\chi_{ij}$.[61] We use values of $a_{ii} = 25$ and $a_{ij} = 40$ that, at a temperature of $k_{\mathrm{B}}T = 1$ and a particle density of $\rho = 3$, corresponds to $\chi_{ij} \approx 4.6$. With an armlength of 8 beads per arm, this gives $\chi N \approx 74$. Due to the many parameters and complexity of a star copolymer melt, parameters for an order–disorder transition are barely existent in the literature. However, a value of $\chi N \approx 74$ is well above the order–disorder transition for diblock copolymers[2] and as high as values used in other studies of ABC star copolymers[5,19] and thus in the strong segregation limit. As a measure of the stretching of the polymer molecules the radius of gyration[62] is provided in the ESI.†

The single beads of the polymer chains are bonded by a harmonic potential, given as $V_{\mathrm{H}}(r) = \frac{1}{2}k(r - r_0)^2$, where k measures the strength of the bond and r_0 the bond rest length. In our system we chose $k = 4\frac{\mathscr{E}}{\mathscr{D}^2}$ and $r_0 = 0.88\mathscr{D}$ as the position of the first peak of the pair correlation function in a system of unbonded, identical particles with the given interaction parameters. Each arm in the polymers consists of 8 beads.

The confinement of the system to a spherical substrate is modelled as follows: the simulation volume is a spherical shell bounded by two repulsive spherical walls interacting with the polymers with a purely repulsive Lennard-Jones potential:

$$V_{\mathrm{LJ}}(r) = 4\varepsilon \left[\left(\frac{\sigma}{r} \right)^{12} - \left(\frac{\sigma}{r} \right)^{6} \right] + \Delta V$$

where r in this case is the length of the vector from the particle perpendicular to the wall, not to be confused with r_{ij}, the pairwise distance between two particles, see Fig. 3. $\Delta V = -(r - r_{\mathrm{cut}})\frac{\partial V}{\partial r}(r_c) - V_{\mathrm{LJ}}(r_c)$ and σ is the range of the repulsive potential, ε would be the strength of the attractive part of the Lennard-Jones potential, however, is of no relevance in the purely repulsive version used here. While the outer wall exerts a force towards its center, the forces of the inner wall acts outwards. Hence, the wall keeps all particle inside the spherical shell they enclose. We choose $\sigma = 1\mathscr{D}$ and set the cutoff of the wall potential to $r_c = 2^{\frac{1}{6}}\sigma$ to cut the attractive tail.

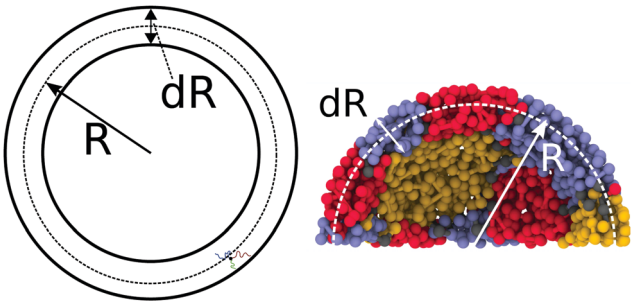

Fig. 3 Simulation setup and substrate model. Left panel: Schematic sketch of a cross section of the simulation setup. The two black, bold circles represent spherical, repulsive 'Lennard-Jones walls' with radii of $R + \frac{\mathrm{d}R}{2} + \sigma$ and $R - \frac{\mathrm{d}R}{2} - \sigma$. As shown, the outer wall exerts a LJ-force on a particle along a vector perpendicular to the wall towards its center. The force of the inner shell acts outwards. Together these walls confine the polymers to a shell of thickness dR. Right panel: Cross section through a simulation snapshot with radius $R = 8\mathscr{D}$ with the same quantities marked. The image shows the homogeneity of structure in the radial direction of the shell and gives an idea for the scale of the system.

The spherical walls are concentric around the origin with radii of $R_i = R - \mathrm{d}R/2 - \sigma$ and $R_o = R + \mathrm{d}R/2 + \sigma$, the shell therefore has a thickness of dR, as shown in Fig. 3. The amount of curvature forced onto the system can then be tuned by varying the radius of the spherical shell. The initial position of the centers of the stars are chosen inside the simulation volume from a uniform distribution. The arms are then placed at random positions around the center. In order to achieve a well mixed configuration the system runs 5.5×10^5 time steps where the interaction parameter between any species of particles is set to $a_{ii} = a_{ij} = 25\frac{\mathscr{E}}{\mathscr{D}}$. After this warmup phase the parameters are set as stated above according to their species. The temperature of the system was kept constant at $k_{\mathrm{B}}T = 1$ for the entire run. All simulations have been run with time steps of $\Delta t = 0.005$ and ran at least 3×10^8 time steps, larger systems with $R > 8\mathscr{D}$ ran 5×10^8 time steps. After these long runs we assume that an equilibrium is reached, which is confirmed visually in random samples. The radius R of the spherical shell was varied with $R = 4, 5, 6, 7, 8, 9, 10\mathscr{D}$ with a shell width of d$R = 2$. Alternating the radius has two effects: (1) due to constant a number density of $\rho = 3\frac{1}{\mathscr{D}^3}$ the number of molecules increase with a larger shell volume; (2) the curvature of the shell decreases with increasing radius. For each radius 20 configurations for each ABC and ABB systems were simulated with different random initialisations for statistical significance.

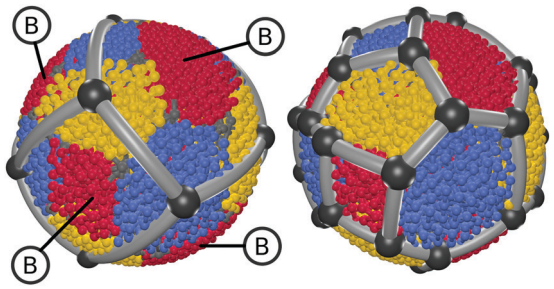

Fig. 4 Two different methods for the analysis of tiling patterns in an ABC system using Set-Voronoi diagrams. Right: Patches of all colors are used to generate a single, three-colored, spherical tiling for a single ABC system. Here the vertices are located at triple lines where three different colors meet and the edges correspond to inter-domain interfaces. The color constraint applies directly to the tiling. Left: Only the patches corresponding to a particular polymeric type X (= A, B, or C) are considered in the tiling analysis, creating a single colored tiling (the image is for X = B, red). The same could be done with the other two colors, yielding in total three single-colored tiling for each ABC system. Note that the color constraint does not apply directly onto this single-colored tiling, *i.e.* uneven numbers of edges are possible, however the frustration on the polymer system still applies. This single-color analysis allows direct comparison to tilings generated in ABB systems, see *e.g.* Fig. 5.

2.2 Structure analysis of tiling patterns

When the simulation is deemed to be equilibrated, the resulting spherical tilings are recovered from the polymer configurations using Set-Voronoi diagrams[63] as implemented in pomelo.[64] The aim is to substitute a domain in the system with a polygon, representing a tile, where the number of edges of the latter is equal to the number of neighboring domains.

In the ABB systems we characterize the structure of the A beads, considering the B particles as a matrix. We use a cluster algorithm (implemented in the trajectory analysis package freud[65]) to identify all A domains. This provides a list of N clusters, one for each A type domain, each with a list of which particles it is made from. Then the Voronoi diagram of all A type particles is computed, where all cells of particles belonging to the same cluster are merged, leaving one cell per cluster. The number of neighbors for each domain are determined from the number of adjacent cells sharing a common edge. The spherical tiling is recovered by representing each domain by a polygon which number of edges equals the number of neighbors.

For the visualizations of the tiling shown in Fig. 5 and 7, the vertices of a tiling are placed at the vertices of the Voronoi cells of the patches. The edges connecting vertices are great circle segments. Fig. 5 shows a simulation snapshot on the left and a representation of the spherical tiling in the middle. We obtain 2D topological representations of the tilings through the Mercator projection as used in.[30] Each point on the sphere given in spherical coordinate angles (θ,ϕ) with $\theta \in [-\pi/2,\pi/2]$ and $\phi \in [0,2\pi]$ is mapped in the Cartesian plane by $x = R\phi$ and $y = R\ln\left(\tan\left(\frac{\pi}{4}+\frac{2}{5}\theta\right)\right)$. An example of such a projection is shown on the right hand panel of Fig. 5. In these representations, the plot has periodic boundary conditions in the x direction, however, not in y direction. The top and bottom tiles therefore are not adjacent, but represent the tiles at the poles of the sphere. The purpose of the planar projections is to correctly capture the topology and neighbor relations, not the geometry, which is deformed in the projection.

In order to make direct comparison to the single-colored tilings from ABB systems to tilings from the ABC systems possible, instead of constructing a three-colored tiling were edges would follow the inter-domain interfaces (see right panel in Fig. 4), we analyse each of the three species in the latter individually, treating the respective other two domains as the matrix, and apply the same analysis as above. That is, to analyse A, we consider B and C indistinguishable and to represent the matrix and so on. From each ABC system three single-colored tilings from the A, B and C type domains are obtained, as can be seen in Fig. 7. In these single-colored tilings the vertices are not restricted to triple-lines and the edges do not correspond to inter-domain interfaces as is

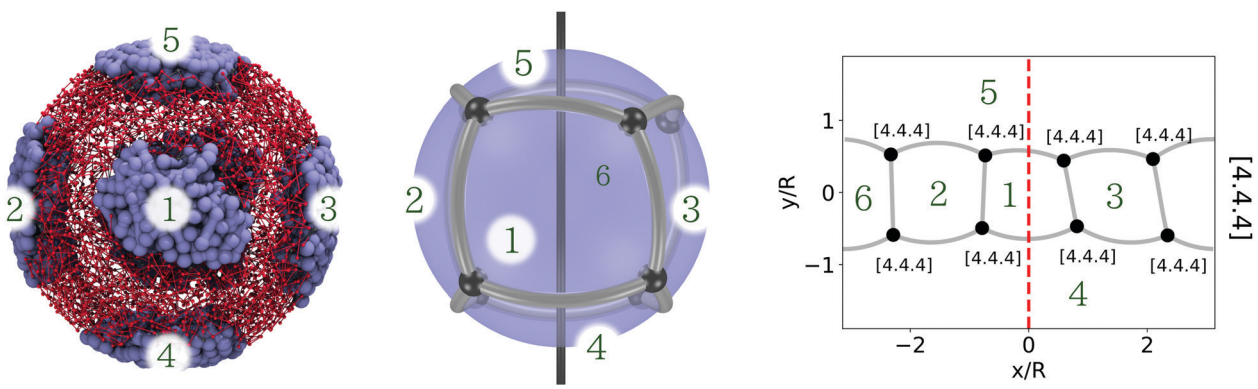

Fig. 5 Spherical tilings from polymeric self-assembly on a spherical substrate. Left panel: A simulation snapshot of an equilibrated ABB star copolymer melt confined to a spherical shell. The A-type arms have assembled into six domains, which arranged in a cuboidal symmetry in the B-type matrix. Middle panel: The spherical tiling recovered from the polymer system. Each face in the tiling corresponds to a blue domain in the simulation snapshot as labeled. Right panel: A modified Mercator projection of the spherical tiling, labeled with the corresponding tiles on the sphere and the domain in the simulation snapshot. Each vertex is labeled with its Schläfli symbol, the union of all types of distinctive vertex labels gives the Schläfli symbol of the entire tiling, as shown vertically on the far right. In order to be comparable, all tilings are rotated so all tilings of a type have the same orientation. The gray axis in the middle panel indicates the orientation of the red, dashed line in the projection in 3D.

This journal is © The Royal Society of Chemistry 2019

the case in ABB systems, see Fig. 4. Although this single-color analysis seems to lift the color constraint of these tilings, *i.e.* polygons with an uneven number of edges are possible, this is a purely virtual aspect of the analysis and the frustration still applies on the polymer systems.

Tilings are labeled using Schläfli Symbols, see caption of Table 1 for details. All simulation screenshots were made using the Tachyon render[66] in VMD,[67] the renderings of the tilings were created using a custom script in BLENDER.[68]

Every 1×10^6 simulation step, a snapshot of all particles was made, which results in 300 frames over the simulation time. The statistics shown in the result section include all tilings from the latest 15 frames of the simulation to account for invalid simulation frames. Since 20 independent runs were made for each radius, 300 frames were analysed for both the ABC and ABB systems. In the ABB system, this provides 300 spherical tilings, in the ABC system 900 tilings, since there are three colors in each frame. Note, however, that the "real" statistics are only based on 20 different runs for each polymer type and radius, since the tiling in the last 15 frames of each run are assumed to be equilibrated and therefore is not expected to change.‡

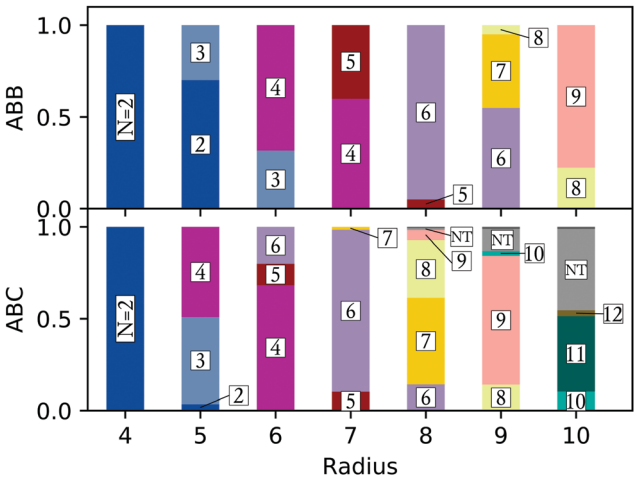

Fig. 6 Equilibrium configurations of self-assembly of star copolymers on a spherical substrate. Results of multiple runs of the self-assembly of ABB (top) and ABC (bottom) star copolymers on a spherical substrate of radius R. Each color denotes one type of tiling, as labeled in Table 1. The plot shows the fraction of simulation snapshots found with the respective tiling for each radius. In general, multiple tilings are found as solutions for a single radius, where the results for ABB and ABC systems differ. The exact data in text form in a table can be found in the ESI.†

3 Results and discussion

We find the following key features:

• For spherical substrates with $R < 8$ all tilings generated by both the ABB and ABC systems are identical to tilings generated from Thomson solutions, see Fig. 6. Only for radii $R \geq 8$, we observed simulations of ABC systems which were not Thomson-type solutions (see below). In ABB systems we only found Thomson solutions.

• For $R > 4$, instead of a single equilibrium solution, we find a spectrum of configurations, see Fig. 6. Within our analysis, these appear as degenerate (or nearly degenerate) configurations that occur with statistical frequencies.

• The analysis of the three single-colored tilings of an ABC system shows that they each individually form Thomson solutions, but not necessarily of the same tessellation type, see Fig. 7.

• The resulting tilings can be tuned by varying the radius of the sphere where the ABC star copolymer system shows a different behaviour in the frequencies of the tilings than the ABB star copolymer systems, see Fig. 6.

To start our discussion we single out the $R = 8$ systems to illustrate the key results. Out of the 300 frames in the ABB systems with $R = 8$, we find the majority of frames (about 95%) to have 6 tiles in a [4.4.4] configuration, only a very small proportions of 5% has 5 tiles in a [3.4.4] tiling. Both of the configurations are identical to tilings generated by Thomson solutions. The ABC case is slightly more complex: out of the 900 analysed tilings, we find only about 14% of the configuration with 6 tiles in a [4.4.4] tiling, 47% with 7 tiles in a [4.4.5] tiling, about 31% with 8 tiles in a [4.4.5, 4.5.5] tiling and 6% with 9 tiles as a [4.5.5, 5.5.5] configuration. As in the ABB systems, all of these are identical to tilings from Thomson solutions. Only about 1% of the tilings were found to differ from the Thomson solution tilings.

While for $R = 8$ the ABB system overwhelmingly forms the same type of tiling, the ABC misses this feature. We find this behaviour across most of the other systems on different radii: all of the ABB systems form at least two different tilings for each radius, the $R = 9$ system even three, however, all are Thomson solutions. All ABC systems show at least three different tilings for each radius, again almost all of them are Thomson solutions. We find exceptions for the $R = 4$ spheres, where for both systems only a single type of tiling is found and the ABC system for $R = 7$, where although three different tilings are found, the majority (86%) of analysed frames forms only one type. Another exception are larger ABC systems, where we find an increasing number ($\approx$1% for $R = 8$, $\approx$12% for $R = 9$, $\approx$44% for $R = 10$) of tilings not connected to the Thomson problem. However, we do see these percentages go down as the simulations are running for longer times so we conjecture that eventually all non-Thomson solutions might anneal out.

Since the free energy levels of different tilings is a function of the sphere radius, as will be discussed later, this may allow the conclusion that the energy levels are almost degenerate for the majority of the combinations of the chosen star copolymers

‡ In general the presented analysis method using Voronoi diagrams works well and is robust. In some rare cases, however, we find it to produce invalid results. These cases are, when very short edges appear in the Voronoi diagram, which means two vertices are very close together. In these cases the neighborhood relations are not clear for the algorithm and small displacements of a single particle can alter the resulting tiling. The other weak point is the cluster analysis. Since all systems are run at finite temperature, there might be particles moving outside their domain in the vicinity of another domains. The cluster algorithm then can mistake both clusters as a single one. Most of these invalid frames can be identified and then ignored by checking if $\chi \neq 2$. A neglectable number of $\approx$1.5% frames were found to be invalid in the sense as discussed.

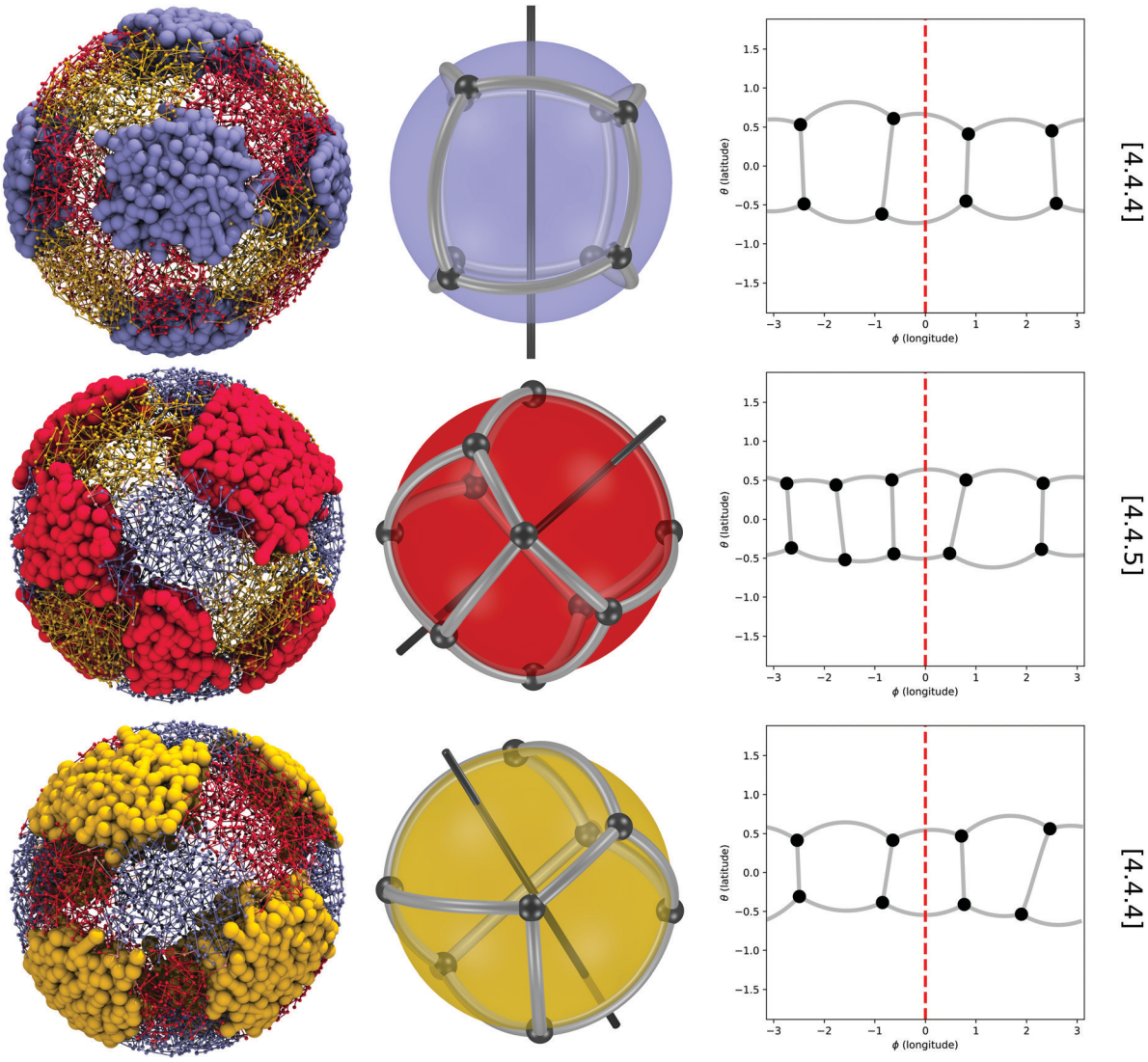

Fig. 7 The three spherical tilings representing the structure of the A, B and C domains. The figure shows three single-colored tilings, generated by the self-assembly of ABC star copolymers, in each of the colors on the same sphere. Left panel: Rendering of the simulation snapshot where the patches creating the tiling are emphasized while showing the others simultaneously. Middle panel: The single-colored tiling derived from the emphasized patch configuration on the left. Note that only patches of the emphasized colors are considered for the computation of the tiling, which allows for direct comparison with single-colored tilings from ABB systems. The axis shows the orientation of the axis with the highest symmetry. Right panel: A 2D projection of the tiling. The black axis in the middle column indicates the position of the red line in the projection plots. The label of the tiling is given on the far right side.

and simulation volume geometry. The finite temperature of our simulation then allows the system to jump into local minima instead of the energetic ground state, which results in the spectrum of tilings found here. For some systems though (R = 4, ABB on R = 7, ABC on R = 8) the energy level of certain configurations seems to be deep enough to prevent other structures to assemble.

For all of the ABB system and ABC systems with $R < 8$ we find that all tilings are of Thomson-type solutions, as seen in Fig. 6. This means that the N A-type (and respectively B- and C-type) patches will sit at the same positions as the electrons would in a N-electron Thomson solution, which we checked by visual observation. This is a remarkable result since although the polymers only have short range interactions a structure of long range order is formed. Such long range interactions in a similar system of interacting micelles formed by diblock copolymers has been predicted by ref. 71.

For ABC systems, with increasing radii beginning at $R \geq 8$ an increasing number of configurations, up to $\approx$40%, are not of the Thomson-type. These are shown in Fig. S2–S9 in the ESI.† An analysis of the patch shapes in Thomson and non-Thomson solutions did not show statistical significant differences. Hence, a correlation between patch shape and being a Thomson or non-Thomson solution could not be found. For more information on the methodology and the data see Fig. S1 in the ESI.† We rather argue that these systems are stuck in local minima.

 This journal is © The Royal Society of Chemistry 2019

The Thomson problem in general is known for its high probability of being stuck in local minima.[40] Already for $N = 32$ electrons the probability of finding the global minimum drops significantly, which roughly coincides with the threshold where our results show local minima. Using polymer melts instead of point-like particles adds even more complexity to the energy landscape. The fact that the ABB systems – somewhat simpler than the ABC system, due to the missing color constraint for example – do not show any non-Thomson solutions and that the proportion of non-Thomson solutions increase with increasing radius, and thus number of patches, supports this.

Based on the observation that the simulations only show Thomson solutions up to systems with $R = 7$, all of those ABC systems must consist of three different tilings, each of which solves the Thomson problem on its own while coexisting with two others on the same sphere. We will elaborate on this again using an example system from the $R = 8$ runs using Fig. 7, however, all systems of various sizes share the same behaviour.

Fig. 7 shows how three different Thomson solutions can coexist on a single sphere. When only considering the blue patches, while red and yellow act as a matrix, the resulting tiling is of type [4.4.4]. Analogue type [4.4.5] and [4.4.4] tilings are formed in the red and yellow patches respectively. The tilings have a different orientation on the sphere as can be seen on the orientation of the axis of highest symmetry.

In the case of the $R = 8$ tilings, the overwhelming number of ABC systems were found to be a combination of three Thomson solutions, where the most prominent combinations are (7/8/8) with 19%, (7/7/8) with 15%, (7/7/7) with 15% and (6/7/7) with 14%. The number denotes the number of patches in the tiling, the tiling label can be found using Table 1. Only a small number of 1% of the systems contained tilings which are not Thomson solutions. The same holds for systems with smaller radius: since no tilings were found not to solve the Thomson problem, all combinations there consist of Thomson solutions. For larger systems the number of non-Thomson configuration increases. Therefore, the amount of configurations containing non-Thomson solutions increases as well, however, we cannot say if that is caused by increasingly difficult equilibration or due to other reasons, for example the color constraint preventing some combinations to be assembled.

In the $R = 8$ case we found the (7/7/7) combination formed in two different ways: once with only Thomson solutions, and once with one Thomson solution and two non-Thomson tilings. In this case we clearly see that it is possible to build this (7/7/7) combination using only Thomson solutions, thus proving that the color constraint does not prohibit the Thomson solutions to form. This hints towards our guess that combinations with non-Thomson solutions are not caused by the color constraint but equilibration issues. Apart from this observation we could not find any regularities in the frequencies of the different combinations of the tilings for any radius.

It is important to note that although the simulation data of ABB systems for $R = 8$ clearly shows the type [4.4.4] tiling as the minimal energy configuration, we could only find one out of 300 combinations being a $3 \times$ [4.4.4] tiling on a single sphere in the ABC systems of the same radius. This observation is found as general behaviour across all runs: there are statistically significant differences in the frequency with which single-colored tilings occur in ABB and ABC systems. This circumstance shows that while the general behavior – forming Thomson solutions – seems untouched by the color constraint, it does affect the self-assembly process: there are differences between ABB and ABC systems that are manifested in the topology of the adopted structures, or at least in the statistical properties of the latter. This observation enables us to answer the following question: if one is only able to see one kind of color, for example by looking through colored filters, is it possible to determine if the observed structure is assembled by an ABB or an ABC system? The answer depends on the circumstances: if only one configuration is available, the answer is no, since each configuration found in this article is assembled by both the ABB and the ABC systems. However, if multiple samples are available, the answer is yes. The different statistics of frequencies of the tilings in the different systems as shown in Fig. 7 enables us to determine the type of systems of the given samples.

To understand why ABC systems behave differently we need to look at the free energy functional determining the resulting structures. When assuming that all equilibrium solutions are Thomson solutions, the resulting tiling type is determined by the number of patches assembled in the melt. As can be seen in the data, this number is a function of the radius: with increasing sphere size the number of patches increases. This follows from the energy functional of polymer melts in the strong segregation limit:

$$F = F_{\mathrm{conf}} + F_{\mathrm{int}}$$

where F_{conf} is the entropic contribution determined by the domain shape and F_{int} is the enthalpic contribution and measures the interface area.[71] The entropic contribution favours most spherical patch shapes and penalises domains, where the polymer chains have to be stretched. Consider an exemplary ABB system with two A-type patches located at the north and south pole of the sphere. The interfaces, on which the grafting points of the star copolymers must sit, are then disk segments centred around the poles. From there the B type arms stretch to cover the entire sphere. Since the arm length is kept constant, the arms must stretch increasingly with increasing sphere radius to cover the surface of the sphere. This comes with an entropic penalty. At some point it becomes energetically more favorable to change to a three patch configuration which, despite the increasing interface energy, relaxes the polymer arms and reduces the entropic energy contribution. This interplay between minimising the interface area and entropic energy contribution determines the number of domains and, thus, the resulting structure in these systems.

The differences in the frequencies of tilings in ABB and ABC systems are caused by a modification of the energy functional. While in the ABB systems only A–B interfaces exist, the ABC systems also develop A–C and B–C interfaces, thus, increasing the enthalpic energy contribution. The entropic contribution changes since the grafting points of the star copolymers are not allowed to move freely along the A–B interface but are constrained to ABC triple lines, resulting in more constrained polymer paths leading, presumably, to an entropic penalty.

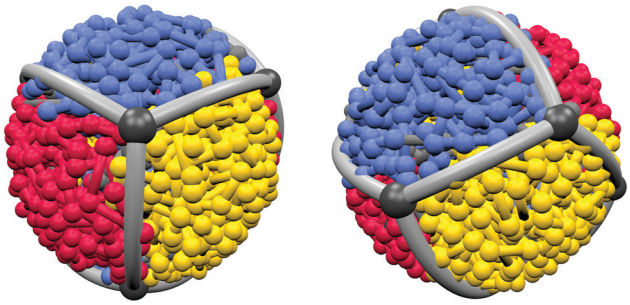

Fig. 8 Rendering and three-colored tiling of a three-colored Thomson solution. The figure shows a three-colored tiling, where each patch of any color corresponds to a Thomson particle. Each color on its own in terms as described above solves the Thomson problem, but also the three-colored tiling solves the Thomson problem. This configuration with $N = 6$ is one of only two where this is possible since the tiling in this case only consists of squares which are allowed with the color constraint.

Apart from the more subtle influences of the color constraint on single-colored tilings in ABC systems, the effect of the color constraint can be directly seen when looking at the three-colored tilings constructed from patches of all colors. In these tilings the vertices and edges of the Voronoi cells coincide with the triple lines and inter-domain interfaces of the polymer structure, see right panel in Fig. 4 or Fig. 8. Note that unlike the single-colored tilings used so far, each patch of any color corresponds to a Thomson particle at once. Here the color constraint can be directly applied to these three-colored tilings. As can be seen in the references in this article, all Thomson solutions for $N \geq 12$ contain tiles with an uneven number of polygons, which means these solutions can not be formed by the polymer melt due to the color constraint. This is backed by our data, where we did not find any of the Thomson solutions for systems with $N \geq 12$, where $N = N_A + N_B + N_C$ is the total number of patches in all colors respectively Thomson particles. For systems with $R \leq 7$ tilings consisting of 6 squares plus $N - 6$ hexagons are found, for system sizes with $R \geq 8$ also octagons occur in tilings with $N \geq 25$. For each octagon an additional square must be introduced to fulfil Eulers equation with $\chi = 2$.

As can be seen in Table 1, the only Thomson solutions for $N < 12$ which only contain polygons with an even number of edges are $N = 3$ and $N = 6$. While the $N = 3$ case proved difficult to equilibrate to a cylindrical phase due to very small system sizes and does not allow for any conclusions, the $N = 6$ case is equivalent to a cube with alternating colored faces and is found for $R = 4$ in ABC systems (see Fig. 8). While each color solves the Thomson problem on its own as single-colored $N = 2$ tilings, the combination of all three colors also forms a three-colored Thomson solution unlike any other configuration in our data. This observation gives rise to the assumption that also for the three-colored tilings the Thomson solutions would be the optimal state, however, the frustration imposed by the color constraint keeps the system in a metastable state.

4 Conclusion and outlook

In this article the self-assembly of ABC and ABB star copolymers confined to a spherical shell was simulated using DPD molecular dynamics simulations in order to investigate the combined influence of geometric frustration and the color constraint inherent in the ABC system. In bulk simulations, these polymers form columnar phases whose cross sections are 3-colored, planar, hexagonal tiling patterns. The architecture of ABC stars imposes the color constraint onto the resulting structures: only tiles with an even number of edges are allowed where the color of all adjacent tiles must alternate. To differentiate between the influence of the color constraint and the curvature ABB systems were simulated as reference, where the color constraint does not apply.

We can summarise our findings into four core results: (1) apart from kinetically stuck configurations in large ABC systems ($R \geq 8$), we find all single-colored tilings in both ABB and ABC systems to be Thomson solutions. (2) In ABC systems we find three possibly different tilings on each sphere, one in each color while neglecting the other two, all of which solve the Thomson problem for small radii individually. We find some non-Thomson solutions for larger radii ($R \geq 8$) but believe this is due to equilibration issues as discussed above.

(3) A spectrum of configurations dominates the ensemble, rather than a single structure. This leads to the occurrence of a small number of different tilings in both ABB and ABC systems, with varying probability. (4) The latter can be tuned by varying the sphere radius, which means we can switch between Thomson solutions of different numbers of particles. While we could not find any combination of three tilings on the same sphere which the color constraint does not allow, the frequencies of the tilings in the ABC compared to the ABB system show statistically significant differences. This provides the possibility to differentiate between the two systems: statistically speaking we can determine if a tiling was formed by an ABB or and ABC system by only being able to see a single color.

A direct comparison of our work to the presented results of frozen particles on a sphere[35] or the diblock copolymers on a spherical substrate[30] is somewhat difficult: while in these systems the number of particles is in the order of 100 (which is equivalent to one patch in our systems), our largest system consists of a maximum of 12 domains in a single tiling. At these system sizes the tilings are missing the regularity to define ''defects'' in their structure. Taking the entire ABC system with all of its colors into account, however, we have a system consisting of up to 37 patches. Here we can see the influence of the color constraint: instead of finding isolated pentagonal defects or scars of pentagons and heptagons, we find either six squares or a combination of squares and octagons to cope with the geometrical constraint.

A promising and interesting application of this work can be found in the field of patchy particles: discrete particles with patches on their surface which can couple and form bonds to other patches, *e.g.* Janus-particles.[72,73] A mechanism to assemble such particles and tune their coordination number include self-assembly of monolayers of surfactants on spherical substrates.[74,75] Our work presents an example how such a self-assembly could be realised. Instead of using two repulsive walls to model a spherical substrate, the architecture and composition of the polymer can be modified, so that spherical droplets will form in solution, as seen

 This journal is © The Royal Society of Chemistry 2019

in previous work.[76–79] Preliminary simulations showed that adding a fourth arm, immiscible with the already existing arms, would form the core of such a droplet, on which surface the ABC arms assemble as presented in this work. By tuning the length of this fourth arm, the radius of the droplets can be changed. As shown in this article, the number of patches would change and therefore the coordination number of the droplet as a patchy particle. Further, instead of using symmetric star copolymers, the length of one arm can be varied to generate different, 'asymmetric' tilings, analogue to.[10,12]

Conflicts of interest

The authors declare no conflict of interest.

Acknowledgements

This work was supported by resources provided by the Pawsey Supercomputing Centre with funding from the Australian Government and the Government of Western Australia, as well as LUNRAC at Lund, Sweden. We thank Nigel Marks from Curtin University, Perth, for fruitful discussions about the Thomson problem.

References

1 F. S. Bates, *MRS Bull.*, 2005, **30**, 525–532.
2 M. W. Matsen, *Self Consistent Field Theory and Its Applications*, Wiley-Blackwell, 2007, ch. 2, pp. 87–178.
3 G. M. Grason and R. D. Kamien, *Macromolecules*, 2004, **37**, 7371–7380.
4 G. Polymeropoulos, G. Zapsas, K. Ntetsikas, P. Bilalis, Y. Gnanou and N. Hadjichristidis, *Macromolecules*, 2017, **50**, 1253–1290.
5 Z. Guo, G. Zhang, F. Qiu, H. Zhang, Y. Yang and A.-C. Shi, *Phys. Rev. Lett.*, 2008, **101**, 028301.
6 C. A. Tyler, J. Qin, F. S. Bates and D. C. Morse, *Macromolecules*, 2007, **40**, 4654–4668.
7 M. G. Fischer, L. de Campo, J. J. K. Kirkensgaard, S. T. Hyde and G. E. Schröder-Turk, *Macromolecules*, 2014, **47**, 7424–7430.
8 S. Okamoto, H. Hasegawa, T. Hashimoto, T. Fujimoto, H. Zhang, T. Kazama, A. Takano and Y. Isono, *Polymer*, 1997, **38**, 5275–5281.
9 J. J. K. Kirkensgaard and S. Hyde, *Phys. Chem. Chem. Phys.*, 2009, **11**, 2016–2022.
10 J. J. K. Kirkensgaard, M. C. Pedersen and S. T. Hyde, *Soft Matter*, 2014, **10**, 7182–7194.
11 J. J. K. Kirkensgaard, *Interface Focus*, 2012, **2**, 602–607.
12 T. Gemma, A. Hatano and T. Dotera, *Macromolecules*, 2002, **35**, 3225–3237.
13 L. de Campo, T. Varslot, M. J. Moghaddam, J. J. K. Kirkensgaard, K. Mortensen and S. T. Hyde, *Phys. Chem. Chem. Phys.*, 2011, **13**, 3139–3152.
14 K. Hayashida, T. Dotera, A. Takano and Y. Matsushita, *Phys. Rev. Lett.*, 2007, **98**, 195502.
15 K. Hayashida, W. Kawashima, A. Takano, Y. Shinohara, Y. Amemiya, Y. Nozue and Y. Matsushita, *Macromolecules*, 2006, **39**, 4869–4872.
16 A. Takano, S. Wada, S. Sato, T. Araki, K. Hirahara, T. Kazama, S. Kawahara, Y. Isono, A. Ohno, N. Tanaka and Y. Matsushita, *Macromolecules*, 2004, **37**, 9941–9946.
17 A. Takano, W. Kawashima, A. Noro, Y. Isono, N. Tanaka, T. Dotera and Y. Matsushita, *J. Polym. Sci., Part B: Polym. Phys.*, 2005, **43**, 2427–2432.
18 P. Tang, F. Qiu, H. Zhang and Y. Yang, *J. Phys. Chem. B*, 2004, **108**, 8434–8438.
19 G. Zhang, F. Qiu, H. Zhang, Y. Yang and A.-C. Shi, *Macromolecules*, 2010, **43**, 2981–2989.
20 Y. Matsushita, *Macromolecules*, 2007, **40**, 771–776.
21 J. J. K. Kirkensgaard, *Phys. Rev. E: Stat., Nonlinear, Soft Matter Phys.*, 2012, **85**, 031802.
22 W. T. M. Irvine, V. Vitelli and P. M. Chaikin, *Nature*, 2010, **468**, 947.
23 W. T. M. Irvine, M. J. Bowick and P. M. Chaikin, *Nat. Mater.*, 2012, **11**, 948–951.
24 R. E. Guerra, C. P. Kelleher, A. D. Hollingsworth and P. M. Chaikin, *Nature*, 2018, **554**, 346.
25 P. Lipowsky, M. J. Bowick, J. H. Meinke, D. R. Nelson and A. R. Bausch, *Nat. Mater.*, 2005, **4**, 407–411.
26 T. Einert, P. Lipowsky, J. Schilling, M. J. Bowick and A. R. Bausch, *Langmuir*, 2005, **21**, 12076–12079.
27 A. R. Bausch, M. J. Bowick, A. Cacciuto, A. D. Dinsmore, M. F. Hsu, D. R. Nelson, M. G. Nikolaides, A. Travesset and D. A. Weitz, *Science*, 2003, **299**, 1716–1718.
28 S. P. Giarritta, M. Ferrario and P. Giaquinta, *Phys. A*, 1992, **187**, 456–474.
29 S. Giarritta, M. Ferrario and P. Giaquinta, *Phys. A*, 1993, **201**, 649–665.
30 L. Zhang, L. Wang and J. Lin, *Soft Matter*, 2014, **10**, 6713–6721.
31 T. L. Chantawansri, A. W. Bosse, A. Hexemer, H. D. Ceniceros, C. J. García-Cervera, E. J. Kramer and G. H. Fredrickson, *Phys. Rev. E: Stat., Nonlinear, Soft Matter Phys.*, 2007, **75**, 031802.
32 R. D. Kamien, *Rev. Mod. Phys.*, 2002, **74**, 953–971.
33 M. J. Bowick and L. Giomi, *Adv. Phys.*, 2009, **58**, 449–563.
34 J. Conway, H. Burgiel and C. Goodman-Strauss, *The Symmetries of Things*, CRC Press, 2016.
35 M. J. Bowick, D. R. Nelson and A. Travesset, *Phys. Rev. B: Condens. Matter Mater. Phys.*, 2000, **62**, 8738–8751.
36 M. Bowick, A. Cacciuto, D. R. Nelson and A. Travesset, *Phys. Rev. Lett.*, 2002, **89**, 185502.
37 M. J. Bowick and Z. Yao, *EPL*, 2011, **93**, 36001.
38 J. J. Thomson, *London, Edinburgh Dublin Philos. Mag. J. Sci.*, 1904, **7**, 237–265.
39 T. Erber and G. M. Hockney, *J. Phys. A: Math. Gen.*, 1991, **24**, L1369.
40 A. N. Bondarenko, M. N. Karchevskiy and L. A. Kozinkin, *J. Phys.: Conf. Ser.*, 2015, **643**, 012103.
41 E. L. Altschuler, T. J. Williams, E. R. Ratner, R. Tipton, R. Stong, F. Dowla and F. Wooten, *Phys. Rev. Lett.*, 1997, **78**, 2681–2685.

42 D. J. Wales and S. Ulker, *Phys. Rev. B: Condens. Matter Mater. Phys.*, 2006, **74**, 212101.
43 D. J. Wales, H. McKay and E. L. Altschuler, *Phys. Rev. B: Condens. Matter Mater. Phys.*, 2009, **79**, 224115.
44 D. L. D. Caspar and A. Klug, *Cold Spring Harbor Symp. Quant. Biol.*, 1962, **27**, 1–24.
45 R. V. Mannige and C. L. Brooks, *Phys. Rev. E: Stat., Nonlinear, Soft Matter Phys.*, 2008, **77**, 051902.
46 S. B. Rochal, O. V. Konevtsova, A. E. Myasnikova and V. L. Lorman, *Nanoscale*, 2016, **8**, 16976–16988.
47 M. Robinson, I. Suarez-Martinez and N. A. Marks, *Phys. Rev. B: Condens. Matter Mater. Phys.*, 2013, **87**, 155430.
48 A. Mughal, *Forma*, 2014, **29**, 13–19.
49 A. Pérez-Garrido, M. J. W. Dodgson and M. A. Moore, *Phys. Rev. B: Condens. Matter Mater. Phys.*, 1997, **56**, 3640–3643.
50 P. J. Hoogerbrugge and J. M. V. A. Koelman, *EPL*, 1992, **19**, 155.
51 P. Español and P. Warren, *EPL*, 1995, **30**, 191.
52 J. J. K. Kirkensgaard, *Soft Matter*, 2010, **6**, 6102.
53 J. J. K. Kirkensgaard, *Soft Matter*, 2011, **7**, 10756.
54 J. A. Anderson, C. D. Lorenz and A. Travesset, *J. Comput. Phys.*, 2008, **227**, 5342–5359.
55 J. Glaser, T. D. Nguyen, J. A. Anderson, P. Lui, F. Spiga, J. A. Millan, D. C. Morse and S. C. Glotzer, *Comput. Phys. Commun.*, 2015, **192**, 97–107.
56 C. L. Phillips, J. A. Anderson and S. C. Glotzer, *J. Comput. Phys.*, 2011, **230**, 7191–7201.
57 R. D. Groot and P. B. Warren, *J. Chem. Phys.*, 1997, **107**, 4423–4435.
58 https://hoomd-blue.readthedocs.io/en/stable/index.html.
59 P. J. Flory, *J. Chem. Phys.*, 1942, **10**, 51–61.
60 M. L. Huggins, *Ann. N. Y. Acad. Sci.*, 1942, **43**, 1–32.
61 R. D. Groot and T. J. Madden, *J. Chem. Phys.*, 1998, **108**, 8713–8724.
62 M. Fixman, *J. Chem. Phys.*, 1962, **36**, 306–310.
63 F. M. Schaller, S. C. Kapfer, M. E. Evans, M. J. Hoffmann, T. Aste, M. Saadatfar, K. Mecke, G. W. Delaney and G. E. Schröder-Turk, *Philos. Mag.*, 2013, **93**, 3993–4017.
64 S. Weis, P. W. A. Schönhöfer, F. M. Schaller, M. Schröter and G. E. Schröder-Turk, *EPJ Web Conf.*, 2017, **140**, 06007.
65 freud, https://freud.readthedocs.io/en/stable/index.html, Accessed: 2019-01-17.
66 J. Stone, MSc thesis, Computer Science Department, University of Missouri-Rolla, 1998.
67 W. Humphrey, A. Dalke and K. Schulten, *J. Mol. Graphics*, 1996, **14**, 33–38.
68 blender, https://www.blender.org/.
69 J. J. K. Kirkensgaard, M. E. Evans, L. de Campo and S. T. Hyde, *Proc. Natl. Acad. Sci. U. S. A.*, 2014, **111**, 1271–1276.
70 B. Grünbaum and G. Shephard, *Tilings and Patterns*, Dover Publications, Incorporated, 2013.
71 A. Semenov, *J. Exp. Theor. Phys.*, 1985, **61**, 744.
72 Z. Zhang and S. C. Glotzer, *Nano Lett.*, 2004, **4**, 1407–1413.
73 C. Casagrande, P. Fabre, E. Raphaël and M. Veyssié, *Europhys. Lett.*, 1989, **9**, 251–255.
74 I. C. Pons-Siepermann and S. C. Glotzer, *Soft Matter*, 2012, **8**, 6226–6231.
75 I. C. Pons-Siepermann and S. C. Glotzer, *ACS Nano*, 2012, **6**, 3919–3924.
76 T. Higuchi, A. Tajima, K. Motoyoshi, H. Yabu and M. Shimomura, *Angew. Chem., Int. Ed.*, 2008, **47**, 8044–8046.
77 T. Higuchi, A. Tajima, H. Yabu and M. Shimomura, *Soft Matter*, 2008, **4**, 1302–1305.
78 S.-J. Jeon, G.-R. Yi, C. M. Koo and S.-M. Yang, *Macromolecules*, 2007, **40**, 8430–8439.
79 K. H. Ku, Y. J. Lee, Y. Kim and B. J. Kim, *Macromolecules*, 2019, **52**, 1150–1157.

This journal is © The Royal Society of Chemistry 2019